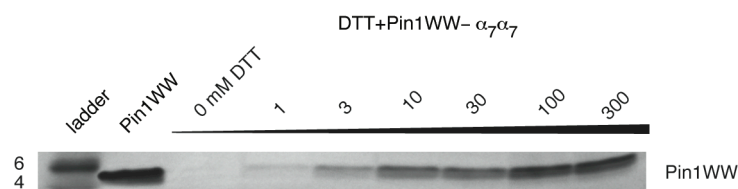


**Figure S1 | Encapsulation of EnHD, Pin1WW and FynSH3 into  $\alpha_7\alpha_7$  or  $\alpha_7\beta_7\beta_7\alpha_7$ .**

**a**, A heterobifunctional cross-linker (LC-SPDP, Pierce) was used to conjugate the N-terminus of the substrate to a cysteine introduced by mutation in  $\alpha$  (S95, R115, or V129).  $\alpha$ -rings were made as a mixture of  $\alpha$ WT and  $\alpha$ -cysteine mutant so that, on average, 1 cysteine mutant (and ultimately 1 substrate molecule) is introduced per chamber. Substrate encapsulation proceeds first by reacting substrate with LC-SPDP, followed by linking to  $\alpha$  by incubation with  $\alpha_7\alpha_7$  or  $\alpha_7\beta_7\beta_7\alpha_7$  under conditions where the substrate is at least 10% unfolded and  $\alpha_7\alpha_7$  /  $\alpha_7\beta_7\beta_7\alpha_7$  is stable (50°C, 100 mM NaCl, 50 mM phosphate, pH 7.5). After overnight incubation of the substrate and  $\alpha_7\alpha_7$  /  $\alpha_7\beta_7\beta_7\alpha_7$  (1.5 substrate – 1  $\alpha_7\alpha_7$  /  $\alpha_7\beta_7\beta_7\alpha_7$ , molar ratios) close to 100% encapsulation efficiencies were observed. Excess substrate was removed by size exclusion chromatography. The conjugation reaction was monitored by SDS PAGE, where a single reaction product was detected, corresponding to the combined masses of  $\alpha$ S95C (~26.1 kDa) and substrate

(EnHD ~7.7 kDa, Pin1WW ~4.4 kDa). Representative gels are shown for encapsulation of EnHD in  $\alpha_7\alpha_7$  (**b**) and Pin1WW in  $\alpha_7\beta_7\beta_7\alpha_7$  (**c**). For specific conjugation between substrate and the linker, the substrate cannot contain lysine sidechains as the linker will react with any primary amine. Therefore substrate lysines were mutated to arginine (in all but one case); this did not compromise the structure or stability of the substrates (data not shown). **d**, The native cysteine of  $\alpha$  at position 151 does not get labeled with substrate. EnHD was incubated with  $\alpha_7\alpha_7$  composed entirely of  $\alpha$ WT under the conditions used in **b** (final lane of the gel in **d**). In this case no cross-linked product ( $\alpha$ -EnHD) was detected (see last lane of gel and note the absence of a peak corresponding to  $\alpha$ -EnHD, compare with EnHD- $\alpha_7\alpha_7$  lane of gel in **b**). Furthermore the intensity of the band corresponding to free EnHD is consistent with the entire amount of EnHD in the reaction. For reference free EnHD was also loaded on the gel in the quantity present in the EnHD,  $\alpha$ WT reaction (3<sup>rd</sup> lane). Therefore the native cysteine of  $\alpha$ WT must be buried in the core of the protein and inaccessible to reaction with the LC-SPDP. Only the cysteines introduced via mutation at positions 95, 115, and 129 are accessible for reaction.



**Figure S2 | Release of the Pin1WW- $\alpha_7\alpha_7$  linker.**

The linker between the substrate and  $\alpha$  contains a disulfide bond which can be released upon addition of reducing agent. To release the substrate linked to  $\alpha_7\alpha_7$ , DTT (1-300 mM) was incubated with Pin1WW- $\alpha_7\alpha_7$  (300  $\mu$ M of the  $\alpha$ -subunit) in 100 mM NaCl, 50 mM phosphate, pH 7.5, for 20 hrs at 25°C. Note,  $\alpha_7\alpha_7$  was composed of a mixture of  $\alpha$ WT and  $\alpha$ S95C to give on average 1  $\alpha$ S95C per  $\alpha_7\alpha_7$  so that 1 substrate molecule is encapsulated per chamber (on average). After incubation the reaction products were separated using a 100 kDa concentrator; Pin1WW- $\alpha_7\alpha_7$  is retained by the membrane, while the released Pin1WW flows through. The flow-through was subsequently analyzed by SDS PAGE. For reference, free Pin1WW was also run (2<sup>nd</sup> lane from left). Increasing amounts of Pin1WW were obtained with increasing amounts of added DTT.

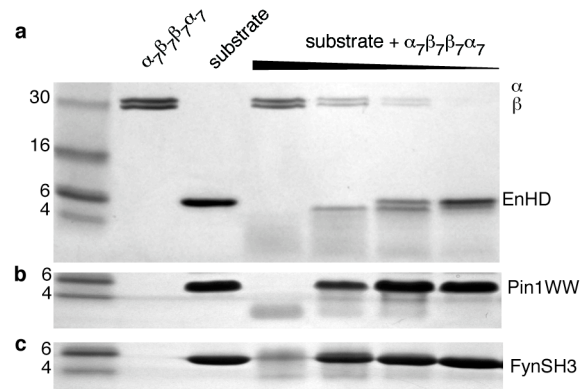


**Figure S3 | EnHD, Pin1WW and FynSH3 are substrates of the WT *T. acidophilum* proteasome.**

500 μM EnHD, Pin1WW, or FynSH3 was incubated with a range of proteasome concentrations (790, 260, 88, and 29 nM in complex) for 16 hrs at 50°C (50 mM NaCl, 25 mM phosphate, pH 6.8). Reactions were quenched by denaturation whereby SDS gel loading buffer was added (2% w/v SDS, 4% v/v glycerol, 40 mM Tris pH 6.8, 0.01% bromophenolblue final concentrations) followed by sample heating (90°C, 10 min). The extent of substrate degradation was assessed by SDS PAGE (Tris-glycine gels with a 4-20% acrylamide gradient), as shown for EnHD (a), Pin1WW (b), and FynSH3 (c). Gel lanes (left to right): molecular weight markers, 790 nM proteasome (no substrate), 500 μM substrate (no proteasome), and 500 μM substrate + proteasome with decreasing concentrations of proteasome (concentrations listed above).

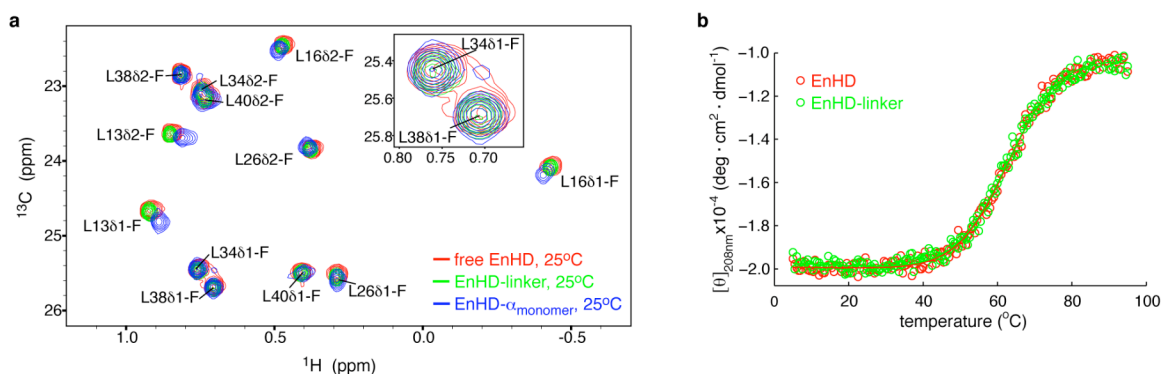


**Figure S4 | The heterobifunctional cross-linker (LC-SPDP) is not responsible for destabilization of EnHD in  $\alpha_7\alpha_7$ .**

**a**, Spectra of the Leu region of free EnHD (red), EnHD-linker (green) and EnHD conjugated to a monomeric version of  $\alpha$  (blue) at 25°C. The spectra of free EnHD and EnHD-linker are indistinguishable, with only very small chemical shift changes in the spectrum of EnHD- $\alpha_{monomer}$  relative to free EnHD and EnHD-linker. It is clear that EnHD- $\alpha_{monomer}$  remains folded (peaks labeled as F) in the context of the  $\alpha$  monomer. Inset shows an expanded region emphasizing that L34 $\delta$ 1, L38 $\delta$ 1 peak positions are superimposable for the three EnHD constructs examined. **b**, Thermal denaturation of EnHD and EnHD-linker as measured by far-ultraviolet CD at 208 nm. Raw data are shown as points with lines indicating fits to the standard equation for two-state unfolding<sup>1</sup>. Melting curves for EnHD and EnHD-linker are indistinguishable, establishing that the linker does not alter the stability of EnHD.

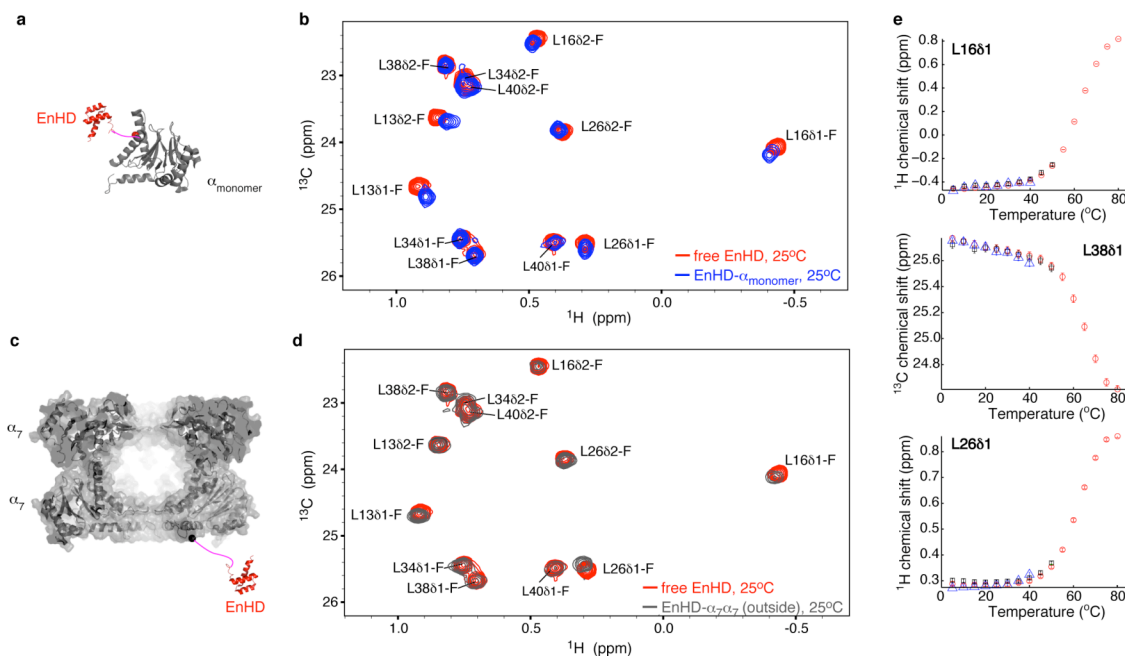


**Figure S5 | EnHD is folded when it is attached to either a monomeric version of  $\alpha$  or to the outside of  $\alpha_7\alpha_7$ .**

**a**, The N-terminus of ILV- $^{13}\text{CH}_3$  EnHD (red) was linked via the heterobifunctional crosslinking reagent, LC-SPDP (magenta), to a cysteine in a monomeric version of  $\alpha$  ( $\alpha_{\text{monomer}}$ , grey), introduced by mutation at position 95 (red sphere). **b**, Leu region of  $^{13}\text{C}$ ,  $^1\text{H}$  correlation maps of free EnHD (red) and EnHD- $\alpha_{\text{monomer}}$  (blue), 25°C, showing that EnHD remains folded (peaks labeled as F) in the context of  $\alpha_{\text{monomer}}$ , with very small chemical shift changes in the spectrum of EnHD- $\alpha_{\text{monomer}}$  relative to free EnHD. **c**, LC-SPDP (magenta) was used to link the N-terminus of ILV- $^{13}\text{CH}_3$  EnHD (red) to the outside of  $\alpha_7\alpha_7$  (grey) at a cysteine introduced by mutation at position 20 (black sphere),  $\alpha\text{R20C}$ . Note,  $\alpha$ -rings were made as a mixture of  $\alpha\text{WT}$  and  $\alpha\text{R20C}$  so that, on average, there is 1 cysteine (1 site of encapsulation) per  $\alpha$ -ring. **d**, Leu region of  $^{13}\text{C}$ ,  $^1\text{H}$  correlation maps of free EnHD (red) and EnHD- $\alpha_7\alpha_7$  (outside, grey), as described in **c**, establishing

that EnHD is folded when it is linked to the outside of  $\alpha_7\alpha_7$ . This is in contrast to when it is conjugated to a position on the inside of  $\alpha_7\alpha_7$  (Figure 1c), where EnHD is unfolded at all temperatures  $\geq 10^\circ\text{C}$  (see Figure S6c). **e**, Temperature dependence of the  $^{13}\text{C}$  or  $^1\text{H}$  chemical shifts of 3 EnHD peaks for free EnHD (red circles), EnHD- $\alpha_{\text{monomer}}$  (blue triangles), and EnHD- $\alpha_7\alpha_7$  (outside) (grey squares). EnHD folding is in the fast exchange regime so the chemical shifts are a population-weighted average of those for the folded and unfolded states. Therefore, the temperature dependence of  $^{13}\text{C}$  or  $^1\text{H}$  chemical shifts can be used to monitor EnHD folding (see main text). Spectra of EnHD- $\alpha_{\text{monomer}}$  and EnHD- $\alpha_7\alpha_7$  (outside) were recorded from 5-40°C and 5-50°C, respectively, reflecting the temperature ranges over which the constructs remained soluble/stable. Clearly the folding behavior of EnHD in the context of these  $\alpha$  constructs is very similar to free EnHD over the measured temperature range.

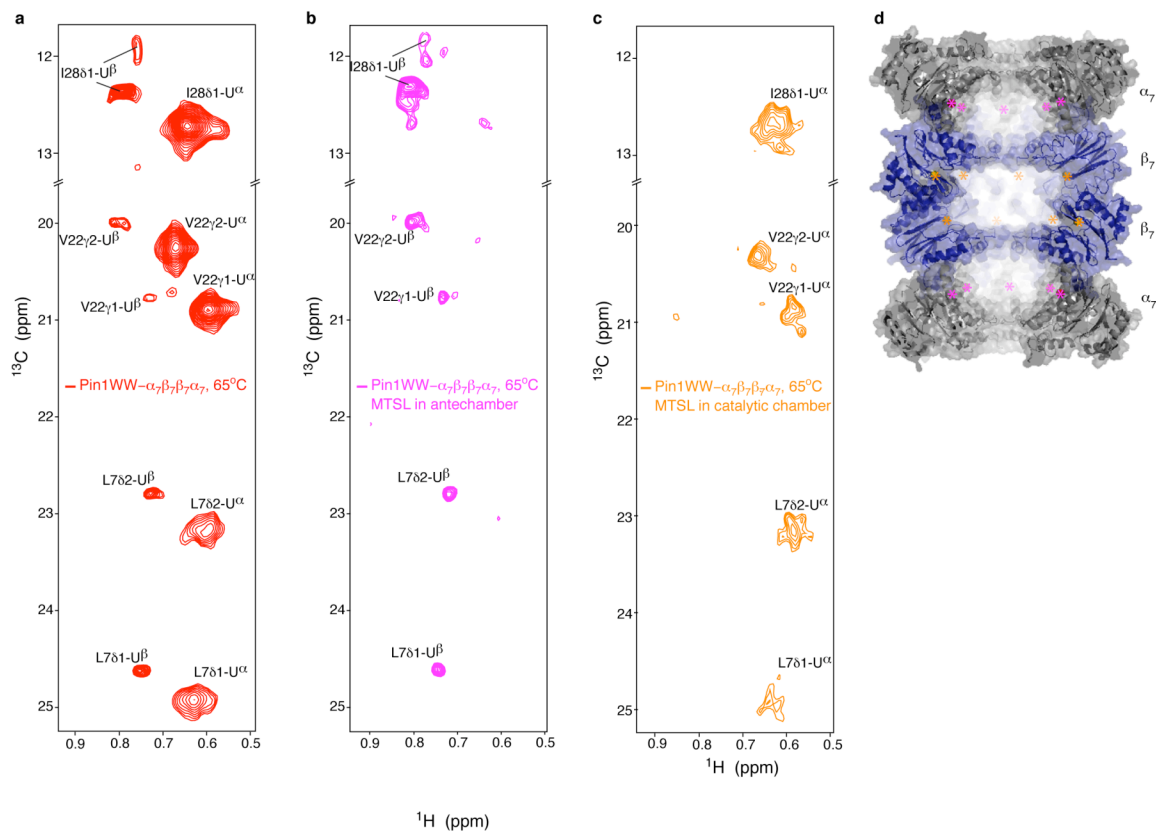


**Figure S6 | Pin1WW is localized to both ante- and catalytic chambers in  $\alpha_7\beta_7\beta_7\alpha_7$ .**

**a**, Spectrum of ILV-methyl labeled Pin1WW in  $\alpha_7\beta_7\beta_7\alpha_7$  at 65°C, where Pin1WW is tethered at residue 95 of  $\alpha$  in the antechamber, with on average 1 Pin1WW domain per antechamber (see Methods). Note that in these  $\alpha_7\beta_7\beta_7\alpha_7$  samples all  $\alpha$  subunits contain the S95C mutation. **b**, Addition of MTSL to the antechamber (at position 95) allows the assignment of sets of peaks in (a) to either the Pin1WW domain in the antechamber (denoted by  $\alpha$ ) or catalytic chamber (denoted by  $\beta$ ). Note that in any antechamber 1 of 7 of component  $\alpha$  subunits is linked with Pin1WW at position 95 (on average) so that the 6 remaining positions are conjugated to MTSL. Addition of MTSL did not disrupt the Pin1WW linkage (data not shown). The peaks that are absent relative to the spectrum in (a) arise from Pin1WW in the antechamber. **c**, Addition of MTSL to G-1C of the pro-sequence in the catalytic chamber (that is inactivated via a T1A mutation) results in



conjugation of spin-label to all 14  $\beta$  subunits in each  $\alpha_7\beta_7\beta_7\alpha_7$  particle and the elimination of peaks arising from Pin1WW localized in the catalytic chamber. **d**, Positions of the spin label in the context of the  $\alpha_7\beta_7\beta_7\alpha_7$  structure. Magenta and orange stars indicate the locations at which the MTSL was attached in  $\alpha$  and  $\beta$  as used for spectra in **(b)** and **(c)**, respectively. The  $\alpha$  and  $\beta$ -rings are colored grey and blue as in Figure 1a of the main text.

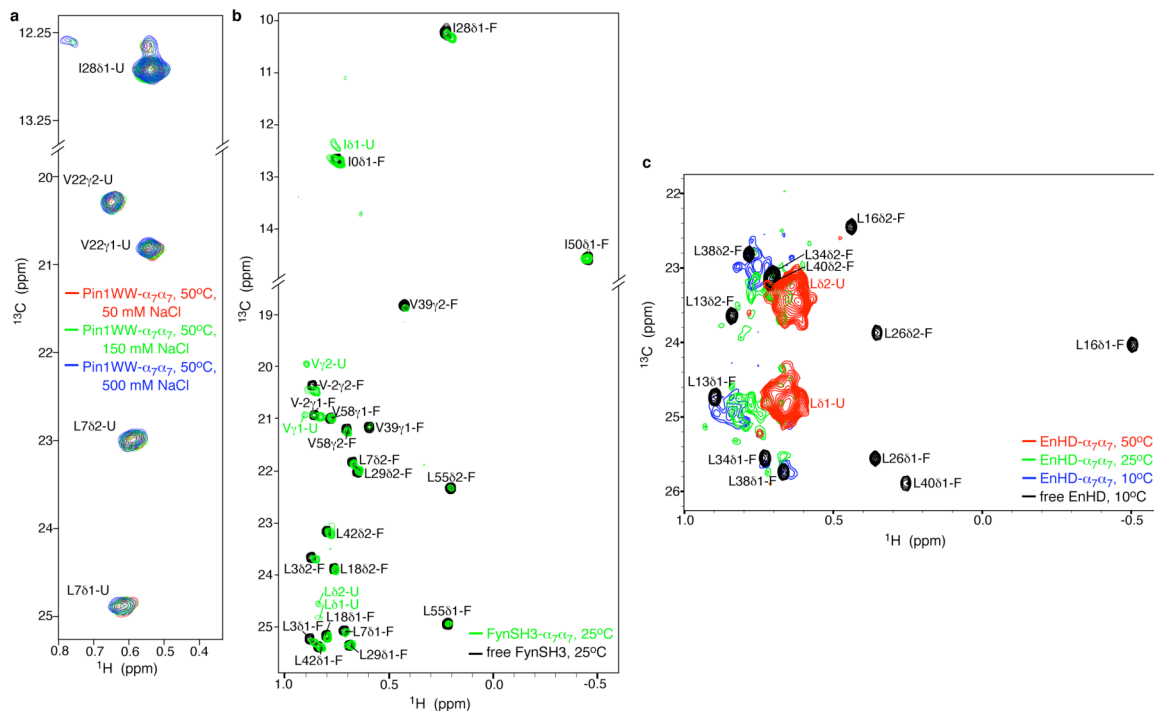


**Figure S7 | Salt and temperature dependence of substrate folding in  $\alpha_7\alpha_7$ .**

**a,**  $^{13}\text{C}$ ,  $^1\text{H}$  HMQC spectra of ILV-methyl labeled Pin1WW in  $\alpha_7\alpha_7$ , 50°C, as a function of NaCl concentration (50 mM, red; 150 mM, green; 500 mM, blue). Spectra are independent of [NaCl] from 50 mM to 500 mM, 50°C, indicating that changes in electrostatics upon encapsulation are not primarily responsible for unfolding.

**b,** Spectra of ILV-methyl labeled FynSH3 in  $\alpha_7\alpha_7$  (green) and free in solution (black) at 25°C. Under these conditions FynSH3- $\alpha_7\alpha_7$  is predominantly folded and the peaks of the folded state (labeled as F) overlay well with those for the free form. Weak intensity peaks corresponding to the unfolded state of FynSH3 are also detected in the spectrum of FynSH3- $\alpha_7\alpha_7$  (labeled as U).

**c,** Spectra of the Leu region of ILV-methyl labeled EnHD encapsulated in  $\alpha_7\alpha_7$  at 50°C (red), 25°C (green) and 10°C (blue). For reference the spectrum of free EnHD, 10°C, is shown (black). At 10°C and 25°C peak clusters from EnHD- $\alpha_7\alpha_7$ , derived from the unfolded state, are observed (that shift with temperature)

while only two weak peaks are positioned close to those for free EnHD, indicating that EnHD- $\alpha_7\alpha_7$  is predominately unfolded at these temperatures, in contrast to Pin1WW- $\alpha_7\alpha_7$  and FynSH3- $\alpha_7\alpha_7$ . All substrates were linked to position 95 of the  $\alpha$ -subunit (1 substrate per chamber).

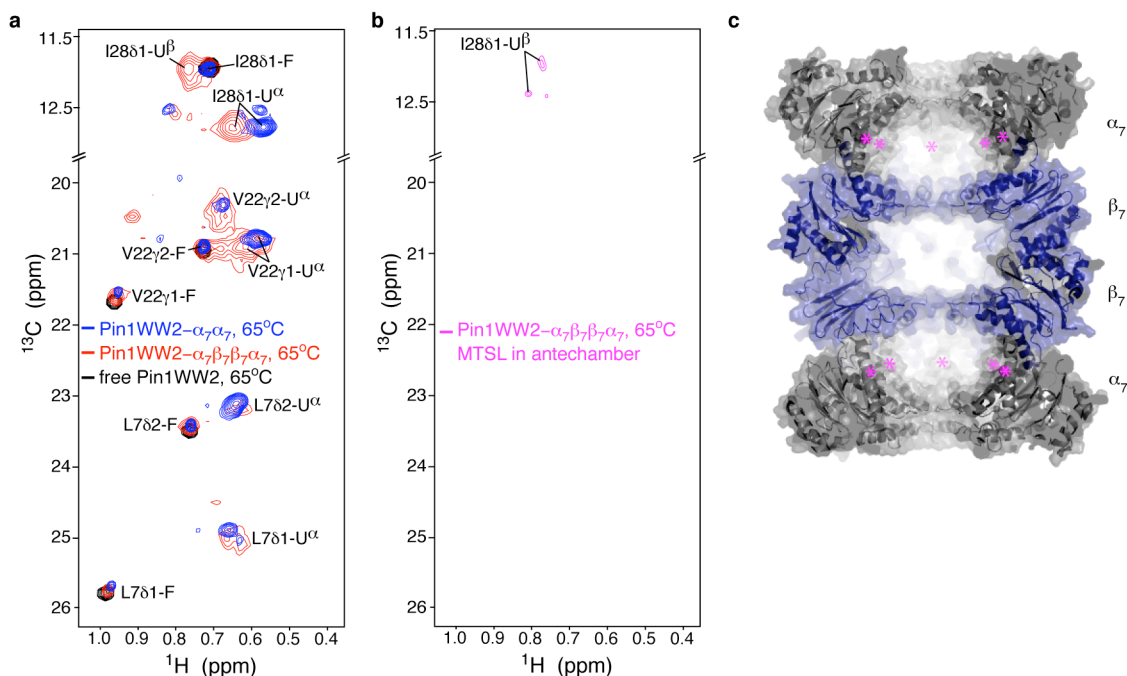


**Figure S8 | The folded and unfolded states of Pin1WW2 reside in the antechamber of  $\alpha_7\beta_7\beta_7\alpha_7$ .**

**a**,  $^{13}\text{C}$ ,  $^1\text{H}$  correlation spectrum of ILV  $^{13}\text{CH}_3$ -Pin1WW2 conjugated at position  $\alpha 95$  in  $\alpha_7\beta_7\beta_7\alpha_7$  at  $65^\circ\text{C}$  (red). Peaks corresponding to folded Pin1WW2 are analogous to free Pin1WW2 at  $65^\circ\text{C}$  (black), whereas peaks corresponding to the unfolded state are analogous to those observed in  $\alpha_7\alpha_7$  (blue). (Pin1WW2 = Pin1WW from human Pin1 with Arg17-Ser18-Ser19 of the WT protein replaced by the two amino acid sequence Ala-Asp that stabilizes the domain, see Fig. S12a). **b**, Addition of MTSL to the antechamber (at position 95), as in Figure S6, allows assignment of sets of peaks in (a) of Pin1WW2 to the antechamber (denoted by  $\alpha$ ). The absence of all peaks corresponding to the Pin1WW2 folded and unfolded states, as reported by the 5 labeled methyl groups, shows that these states are associated with encapsulation in the antechamber. However, two peaks in the Ile region of the spectrum remain. These peaks derive from the Pin1WW2 in the catalytic chamber (denoted by  $\beta$ ) as they have the same chemical shifts

as Pin1WW (WT) in the catalytic chamber of  $\alpha_7\beta_7\beta_7\alpha_7$  at 65°C (Figure S6). **c**, Positions of the spin label are indicated with magenta stars in the context of the  $\alpha_7\beta_7\beta_7\alpha_7$  structure.

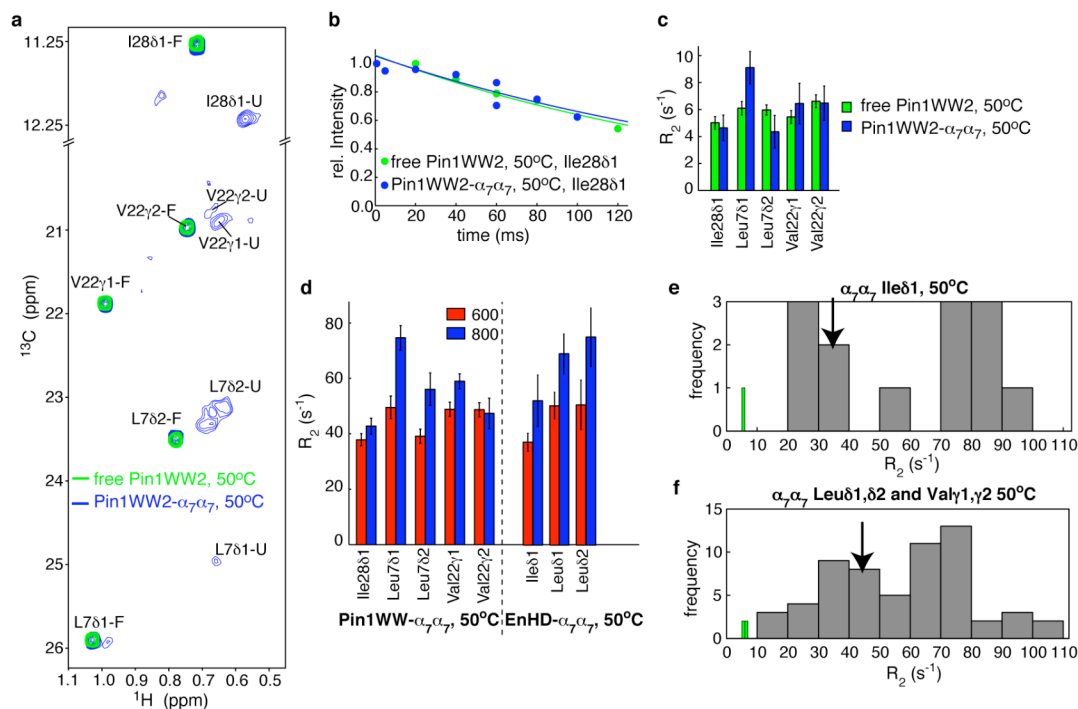


**Figure S9 | Pin1WW2 is predominately folded when encapsulated in  $\alpha_7\alpha_7$  at 50°C and in the folded state does not interact with the cavity walls.**

**a**,  $^{13}\text{C}$ ,  $^1\text{H}$  HMQC spectrum of ILV-methyl labeled Pin1WW2 in  $\alpha_7\alpha_7$ , 50°C (blue), with the spectrum of the free Pin1WW2 shown for comparison (green). Pin1WW2 is a stabilized mutant of Pin1WW, Fig. S12a. The melting temperatures for WT Pin1WW and Pin1WW2 are 59°C and 77.5°C, respectively<sup>2</sup>. **b-c**,  $^1\text{H}$   $R_2$  rates for the slowly relaxing methyl proton transitions<sup>3</sup> of free (green) and  $\alpha_7\alpha_7$  (blue) encapsulated Pin1WW2 50°C, 600 MHz (quantified from the peaks corresponding to the folded state). Representative experimental decay curves (circles) from which  $^1\text{H}$   $R_2$  rates for the Ile28 $\delta$ 1 methyl group are extracted based on fits to an exponential (solid curve) are shown in **(b)** along with  $^1\text{H}$   $R_2$  rates for all I,L,V methyl groups of Pin1WW2 in **(c)**. By comparison,  $R_2$  rates have been measured for Pin1WW- $\alpha_7\alpha_7$  and EnHD- $\alpha_7\alpha_7$  (50°C, 600 and 800 MHz, only the unfolded states are observed for these substrates) that are much larger than the

corresponding values for the folded state of the encapsulated Pin1WW2 (**d**). This is to be expected since, unlike the folded domain of the encapsulated Pin1WW2, both Pin1WW and EnHD interact with the walls of the cavity at 50°C. The dependence of  $^1\text{H}$   $R_2$  on field strength for some residues indicates that millisecond exchange processes contribute to relaxation. **e-f**, Distribution of  $^1\text{H}$   $R_2$  rates in  $\alpha_7\alpha_7$  for Ile $\delta$ 1 (**e**) and Leu, Val (**f**) methyl groups measured at 50°C and at a field strength of 600 MHz (grey bars). The distribution of  $R_2$  rates for free Pin1WW is also shown at 50°C, 600 MHz (green bars). Black arrows designate  $^1\text{H}$   $R_2$  rates measured for I,L,V methyl groups of encapsulated EnHD, 50°C (values shown in (**d**)). Note that for EnHD in  $\alpha_7\alpha_7$  the unfolded state peaks are overlapped and cannot be reliably decomposed. Therefore intensities were measured by numerically summing over each peak cluster and reported relaxation rates are qualitative. Only one of each of Ile, Leu and Val is present in Pin1WW and Pin1WW2 so that this is never a problem for these proteins.

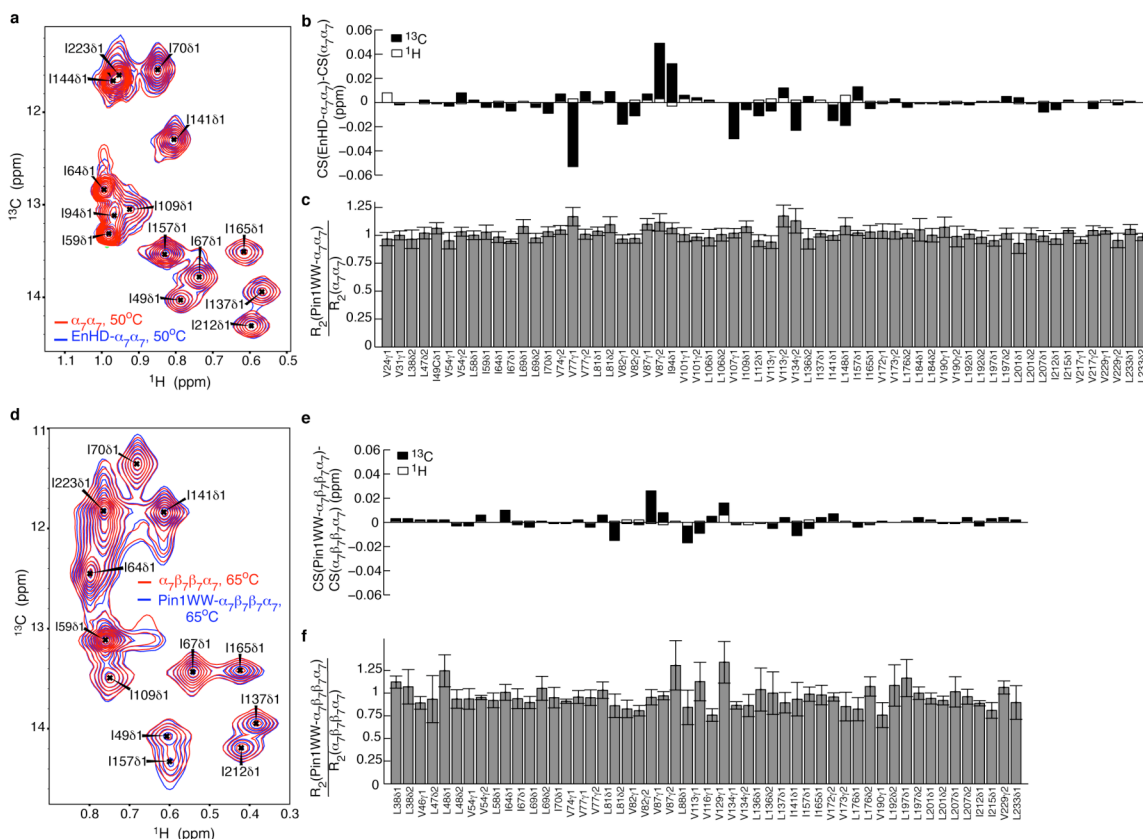


**Figure S10 | The chemical shifts and transverse relaxation rates of  $\alpha$  methyl groups change little upon encapsulation of protonated substrate in  $\alpha_7\alpha_7$  or  $\alpha_7\beta_7\beta_7\alpha_7$ .**

**a-c,** Effect of encapsulating EnHD in  $\alpha_7\alpha_7$ . **a,** Representative region of the  $^{13}\text{C}$ ,  $^1\text{H}$  HMQC spectrum of ILV methyl labeled  $\alpha$  in  $\alpha_7\alpha_7$  with (blue) and without (red) encapsulated EnHD, 50°C. **b,** Quantitation of changes in carbon (black) and proton (white) chemical shifts upon encapsulation of EnHD for all peaks in the spectrum. **c,** Ratio of the  $^1\text{H}$   $R_2$  rates for the slowly relaxing methyl proton transitions<sup>3</sup> of  $\alpha$  in  $\alpha_7\alpha_7$ -EnHD relative to  $\alpha_7\alpha_7$  at 50°C, 600 MHz. Note only non-overlapping peaks were quantified. **d-f,** Effect of encapsulating Pin1WW in  $\alpha_7\beta_7\beta_7\alpha_7$  on  $\alpha$  methyl groups. Parts **(d)**, **(e)**, and **(f)** are analogous to **(a)**, **(b)**, and **(c)**, respectively. Note that fewer peaks could be quantified in spectra recorded of  $\alpha_7\beta_7\beta_7\alpha_7$  relative to  $\alpha_7\alpha_7$  because of the poorer quality of the data obtained for the full proteasome. In both **(b)** and **(e)** the chemical shift



changes are very small establishing that either  $\alpha$  does not change conformation, or that structural changes are minor, upon encapsulation of substrate into  $\alpha_7\alpha_7$  or  $\alpha_7\beta_7\beta_7\alpha_7$ . Moreover, the relaxation properties do not significantly change, indicating that the dynamics are also not affected. It is also worth noting that spectra of  $\alpha_7\alpha_7$  or  $\alpha_7\beta_7\beta_7\alpha_7$  containing cys mutants for tethering substrate (in  $\alpha$ -subunits) or mutations rendering the full length proteasome inactive (in  $\beta$ -subunits) were also very similar to spectra of the wild-type constructs.

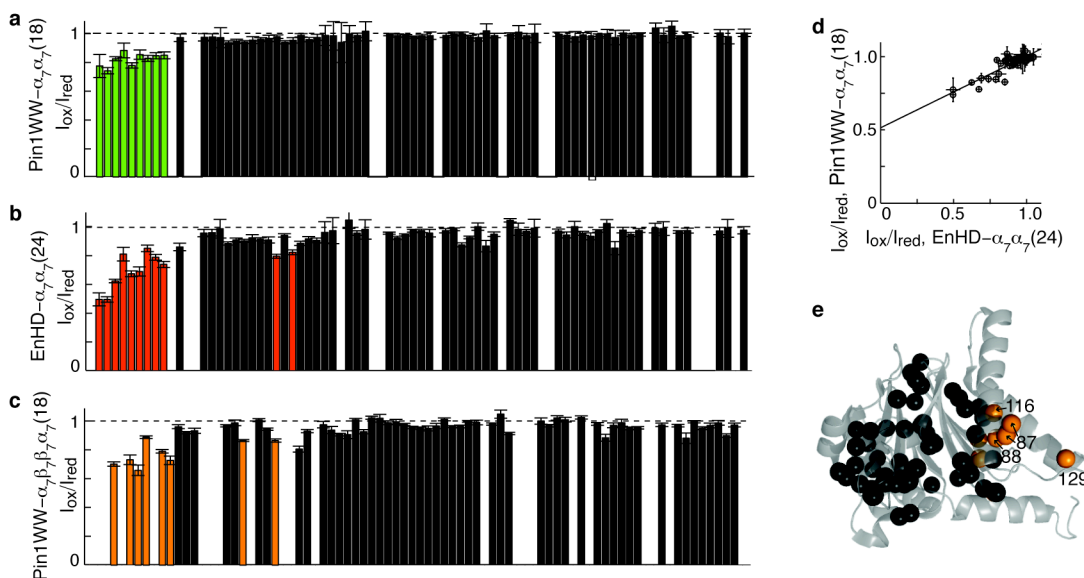


**Figure S11 | Effects of substrate-spin labels on intensities of  $\alpha$  methyl peaks.**

**a-c**, Attenuation of cross-peaks in HMQC spectra recorded on ILV-methyl labeled  $\alpha_7\alpha_7$  (50°C) or  $\alpha_7\beta_7\beta_7\alpha_7$  (65°C) resulting from attachment of a TEMPO nitroxide spin label to residue 18 of Pin1WW encapsulated in  $\alpha_7\alpha_7$  (**a**), to residue 24 of EnHD in  $\alpha_7\alpha_7$  (**b**) or to residue 18 of Pin1WW in  $\alpha_7\beta_7\beta_7\alpha_7$  (**c**). Note that the methyl groups are arranged in order of their proximity to the chamber ‘inside’ surface (left to right, groups are located increasingly farther from the surface). Groups with >10% decrease in the intensity ratio are colored in green for Pin1WW- $\alpha_7\alpha_7$ (18), in red for EnHd- $\alpha_7\alpha_7$ (24) and in orange for Pin1WW- $\alpha_7\beta_7\beta_7\alpha_7$ (18). Shown are intensity ratios obtained by recording spectra either with TEMPO-labeled  $^1\text{H}$  substrate ( $I_{ox}$ ) or with  $^1\text{H}$  substrate ( $I_{red}$ ), see below. **d**, Comparison of intensity ratios for TEMPO-labeled EnHD and Pin1WW in  $\alpha_7\alpha_7$ . The pattern of intensity changes for spin-labeled EnHD and Pin1WW are similar (correlation coefficient=0.90) but the extent of attenuation is generally less for Pin1WW), consistent with the spin-label occupying more locations closer to the surface of the cavity when attached to EnHD and suggesting that EnHD interacts more strongly with the surface

than Pin1WW. **e**, Positions with the greatest changes in peak intensities for Pin1WW- $\alpha_7\beta_7\beta_7\alpha_7$ (18) are indicated in the context of the structure of the proteasome antechamber, with changes  $>10\%$  ( $<10\%$ ) shown as orange (black) spheres. The orientation of  $\alpha$  is the same as in Figure 3b. The changes are qualitatively very similar to what was quantified for  $\alpha_7\alpha_7$ , **a**, with methyl residues exhibiting the greatest reduction in intensity upon encapsulation of spin-labeled Pin1WW residing near the inside surface of the  $\alpha$ -ring, just as with  $\alpha_7\alpha_7$ . The slight differences in the PRE profiles reflects the poorer data quality in the case of the full proteasome (absence of peaks or overlap), despite the fact that experiments were performed at  $65^\circ\text{C}$  to offset the increase in molecular weight of the larger particle relative to  $\alpha_7\alpha_7$ . It is noteworthy that intensity changes are only observed for methyl groups located near the inside surface of  $\alpha$ -ring, indicating that it is highly unlikely that Pin1WW leaves the antechamber via the annulus (Figure 1) or dynamic side pores.

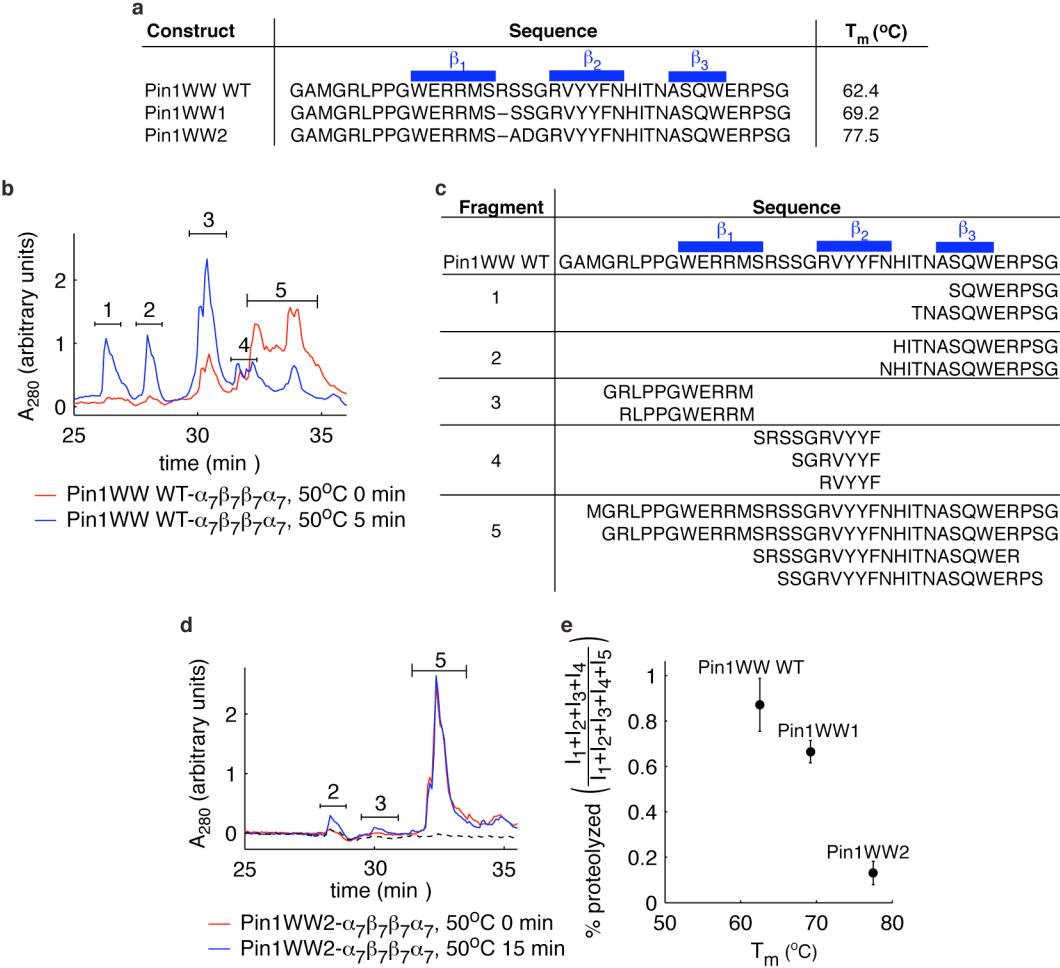


**Figure S12 | Substrate stability correlates inversely with its proteolysis.**

In order to demonstrate that maintaining substrates in an unstructured state inside the antechamber of the proteasome promotes proteolysis, we have measured the hydrolysis of a number of different constructs of the Pin1 WW domain, including WT Pin1WW (referred to as Pin1WW in the text and SI figures) and a pair of stabilized mutants of the Pin1WW domain, Pin1WW1 and Pin1WW2. Proteolysis assays (see below) were carried out using proteasomes that were constructed from  $\alpha$ -subunits containing the S95C mutation and WT  $\beta$ -subunits. Proteasomes, deactivated with the inhibitor Calpain Inhibitor I (4  $\mu$ M proteasome, 5 mM Calpain Inhibitor I,  $K_i$ =~500 nM (ref 4)), were

loaded with Pin1WW constructs of varying stabilities by cross-linking to the wall of the antechamber at position 95; on average a single substrate was tethered to each antechamber. Loading was achieved by adding 10-fold molar excess substrate over proteasome and incubating at elevated temperature (65°C for Pin1WW WT, 72°C for Pin1WW1, and 80°C for Pin1WW2). Substrate was subsequently released from the tether by first cooling to 5°C (presumably resulting in folding of substrate), and incubating with 0.5 M DTT for 2 hours. Next, to simultaneously activate proteasomes by removing inhibitor and to remove unencapsulated substrate, the reaction was buffer exchanged using a concentrator (MW cutoff = 100 kDa, 5°C). Proteolysis was then allowed to occur by incubation of the substrate- $\alpha_7\beta_7\beta_7\alpha_7$  complex at 50°C for 5 or 15 min. Reactions were quenched upon addition of 6 M Gdn-HCl acidified with 1% TFA, denaturing both proteasome and substrate, and samples were kept frozen until analyzed by reverse phase (RP) HPLC to separate reaction products. Figures **a** and **e** have been repeated from Figure 4 of the main text for clarity.

**a**, Primary sequence of the WW constructs used in this assay, with  $T_m$  values (free form) as indicated<sup>2</sup>. The locations of  $\beta$ -strands are highlighted.

**b,c** RP HPLC elution profiles (monitored at 280 nm) for the Pin1WW WT- $\alpha_7\beta_7\beta_7\alpha_7$  reaction immediately after inhibitor and excess Pin1WW WT was removed (red, 0 min) and after 5 min incubation at 50°C (blue). Note that peaks for proteasome  $\alpha$  and  $\beta$  were also detected but were well resolved from Pin1WW WT (not shown). The content of the 5 major Pin1WW WT peak groups was determined using MALDI mass spectrometry (**c**). A small amount of degradation is observed at the zero time-point (small amount of peak 3, red, and 4 which does not resolve from 5), however very significant levels of degradation are noted after 5 minutes, 50°C (build-up of peaks 1-4, blue). Two

experiments establish that substrate exit and re-entry into different proteasomes does not contribute to the degradation profile at least on a scale of 5 min: (1) After 5 minutes incubation little intact substrate remains. Virtually all of the WW reaction products are outside the proteasome, as assayed by the flow-through from a 100kDa concentrator that retains the proteasome. However, additional incubation (10 more min) at 50°C does not change the degradation profile (data not shown), suggesting that the products do not re-enter the proteasome and undergo further degradation. (2) The observed degradation profile is independent of the concentration of the Pin1WW WT- $\alpha_7\beta_7\beta_7\alpha_7$  complex (data not shown). Note that degradation of encapsulated WW domain is independent of the concentration of Pin1WW WT- $\alpha_7\beta_7\beta_7\alpha_7$ , while proteolysis that proceeds by entrance of substrate that has escaped the proteasome at some earlier stage would be expected to be a function of the concentrations of substrate and  $\alpha_7\beta_7\beta_7\alpha_7$ . The fact that a concentration dependence was not noted establishes that the degradation profiles reflect proteolysis of substrate that remains encapsulated for the duration of the reaction.

**d**, RP HPLC elution profiles (280 nm) for Pin1WW2- $\alpha_7\beta_7\beta_7\alpha_7$  complex immediately after inhibitor and excess Pin1WW2 is removed (red, 0 min) and after 15 min incubation at 50°C (blue). The profile is little changed, establishing that Pin1WW2 does not get degraded over a time-scale that is three-fold longer than for Pin1WW WT where excessive proteolysis has occurred. Pin1WW2 remains inside the proteasome, as it is not present in the flow-through from a 100kDa concentrator used to separate free Pin1WW2 from the proteasome (black, dashed line).

**e**, Correlation between  $T_m$  of the free substrate and extent of substrate proteolysis. Proteolysis of (Pin1WW WT, Pin1WW1, and Pin1WW2) was measured at 50°C after (5 min, 5 min, 15 min) incubation. Note that the extent of proteolysis, as measured by the relative peak areas,  $1+2+3+4 / 1+2+3+4+5$ , does not change for Pin1WW WT and Pin1WW1 between 5 and 15 min (data not shown), reflecting the fact that there are

preferential cleavage sites in the WW domain and that these are already cleaved for Pin1WW WT and Pin1WW1 after 5 min. Substrate  $T_m$  values are decreased upon encapsulation into  $\alpha_7\beta_7\beta_7\alpha_7$  with all three substrates having different relative populations of unfolded / folded states, as established by NMR studies (50°C) described in the text. The inverse correlation between substrate stability and extent of proteolysis implies that the proteasome processes unfolded substrate more efficiently than folded substrates due to either an increased rate of translocation into the catalytic chamber and/or an increase in the chemical step of hydrolysis. Our data do not allow us to distinguish between these possibilities.

Peak	% Folded	
	$\alpha_7\beta_7\beta_7\alpha_7$	$\alpha_7\alpha_7$
I28 $\delta$ 1	29.9 $\pm$ 4.9	30.2 $\pm$ 3.8
V22 $\gamma$ 1	32.1 $\pm$ 8.3	31.8 $\pm$ 4.5
V22 $\gamma$ 2	23.3 $\pm$ 9.5	27.1 $\pm$ 10.3
L7 $\delta$ 1	17.8 $\pm$ 10.5	20.8 $\pm$ 4.0
L7 $\delta$ 2	29.9 $\pm$ 9.5	26.2 $\pm$ 3.4

**Table S1 | The populations of the folded state of Pin1WW2 encapsulated in  $\alpha_7\beta_7\beta_7\alpha_7$  and in  $\alpha_7\alpha_7$ , 65°C, are nearly identical.**

Quantitation of the fraction of Pin1WW2 folded at 65°C in  $\alpha_7\beta_7\beta_7\alpha_7$  and  $\alpha_7\alpha_7$ , computed for each labeled methyl group from the peak intensities of the folded and unfolded states (Figure S8). Pin1WW2 is destabilized to a similar extent in  $\alpha_7\beta_7\beta_7\alpha_7$  and  $\alpha_7\alpha_7$ . For reference, free Pin1WW2 is 85% folded under these conditions.

References

1. Fersht *Structure and Mechanism in Protein Science* (W H Freeman & Co, 1999).
2. Jäger, M., Zhang, Y., Bieschke, J., Nguyen, H., *et al.* Structure-function-folding relationship in a WW domain. *Proc. Natl. Acad. Sci. U S A* **103**, 10648-10653 (2006).
3. Tugarinov, V. & Kay, L. E. Relaxation rates of degenerate 1H transitions in methyl groups of proteins as reporters of side-chain dynamics. *J. Am. Chem. Soc.* **128**, 7299-7308 (2006).



4. Huffman, H. A., Sadeghi, M., Seemuller, E., Baumeister, W. & Dunn, M. F. Proteasome-cytochrome c interactions: a model system for investigation of proteasome host-guest interactions. *Biochemistry* **42**, 8679-8686 (2003).